



HAL
open science

Dynamics of turbulent boundary layers exciting wavepackets in subsonic jets

Oguzhan Kaplan, Peter Jordan, André Cavalieri, Guillaume A Brès

► **To cite this version:**

Oguzhan Kaplan, Peter Jordan, André Cavalieri, Guillaume A Brès. Dynamics of turbulent boundary layers exciting wavepackets in subsonic jets. 25th AIAA/CEAS Aeroacoustics Conference, May 2019, Delft, Netherlands. 10.2514/6.2019-2567 . hal-02378557

HAL Id: hal-02378557

<https://hal.science/hal-02378557>

Submitted on 25 Nov 2019

HAL is a multi-disciplinary open access archive for the deposit and dissemination of scientific research documents, whether they are published or not. The documents may come from teaching and research institutions in France or abroad, or from public or private research centers.

L'archive ouverte pluridisciplinaire **HAL**, est destinée au dépôt et à la diffusion de documents scientifiques de niveau recherche, publiés ou non, émanant des établissements d'enseignement et de recherche français ou étrangers, des laboratoires publics ou privés.

Dynamics of turbulent boundary layers exciting wavepackets in subsonic jets

Oğuzhan Kaplan^{*†}, Peter Jordan[‡], André V. G. Cavalieri[§] and Guillaume A. Brès[¶]

Azimuthally coherent low-energy structures in the form of wavepackets are documented to play dominant role in sound radiation by subsonic turbulent jets. In earlier work, we have shown evidence of a coupling between the turbulent nozzle boundary-layer (NBL) disturbances and wavepackets in a $M=0.9$ turbulent jet, by means of two point statistics.¹ The purpose of this study is to characterise the structures within the NBL using a high-fidelity large-eddy simulation of a $M=0.4$ turbulent jet. We first employ Spectral Proper Orthogonal Decomposition (SPOD) to the axisymmetric component of the flow in order to distill a low-rank approximation of the flow dynamics. This reveals the existence of coherent structures within the NBL and shows that these are correlated with wavepackets in the jet. We then model the NBL structures via a mean-flow stability analysis. Projection of the leading SPOD modes on the stability eigenmodes shows that the organised boundary layer structures can be modelled using a small number of stable eigenmodes. Finally local resolvent analysis of the mean-flow is performed. It is shown that the most-energetic nozzle structures can be successfully modelled with optimal resolvent response modes.

Nomenclature

m	Azimuthal mode number	Re	Reynolds number
ω	Angular frequency	St	Strouhal number
α	Angular wavenumber	U_j	Mean streamwise jet exit velocity
t_{sim}	Total simulation time	ν	Kinematic viscosity
Δt	Sampling time	<i>Subscript</i>	
c_∞	Speed of sound	*	Dimensional quantity
D	Jet diameter	∞	Freestream property

I. Introduction

Numerous studies have shown that turbulent jet dynamics contain axially elongated, azimuthally organised coherent structures, wavepackets, which play a key role in turbulent jet noise.²⁻⁵ The principle hallmarks of wavepackets can be modeled by solving the linearised Navier-Stokes equations.^{6,7} But questions remain regarding the mechanism by which the wavepacket amplitudes are set. The goal of this study is to provide clarification on this point.

Previous studies have shown that nozzle boundary-layer conditions influence both noise generation and downstream jet dynamics,^{8,9} but further analysis is required to explore the importance of nozzle boundary

^{*}Graduate Student, Département Fluides, Thermique et Combustion, Institut Pprime, CNRS, Université de Poitiers, EN-SMA, 86000 Poitiers, France

[†]Teaching Assistant, Univ. Lille, CNRS, ONERA, Arts et Metiers ParisTech, Centrale Lille, FRE 2017 - Laboratoire de Mécanique des fluides de Lille - Kampé de Fériet, F-59000 Lille, France

[‡]Research Scientist, Département Fluides, Thermique et Combustion, Institut Pprime, CNRS, Université de Poitiers, EN-SMA, 86000 Poitiers, France

[§]Assistant Professor, Divisão de Engenharia Aeronautica, Instituto Tecnológico de Aeronautica, 12228-900 São Jose dos Campos, SP, Brazil

[¶]Senior Research Scientist, Cascade Technologies Inc., Palo Alto, CA 94303

layer dynamics. We address the question as to what kind of framework is needed to model nozzle boundary-layer (NBL) structures.

Spectral proper orthogonal decomposition (SPOD), first proposed by Lumley,¹⁰ is a practical tool for educing coherent structures in turbulent flows, and has been employed extensively in the analysis of numerical and experimental data in turbulent jets.^{11–14} We use SPOD to identify coherent structures within the nozzle and in the jet, and to seek a connection between the two regions. The results reveal axisymmetric coherent structures in the nozzle boundary-layer, and shows that these are linked to the wavepackets in the jet.

Motivated by the success of linear theory in modelling the wavepackets downstream of the jet exit, we use linear theory to model the NBL structures. Projection of the most-energetic axisymmetric NBL structures, which SPOD analysis reveals to be connected to the downstream wavepackets, onto a family of discrete eigenmodes enables identification of the amplitudes of the eigenmodes. Using a small number of eigenmodes the NBL dynamics can be reproduced with reasonable accuracy.

Finally, we perform an input-output analysis using the resolvent of the linearised Navier-Stokes operator. We compare resolvent response modes, which are computed in locally parallel framework, to the NBL wavepackets identified through SPOD. Results demonstrate that the resolvent modes describe the local features of the NBL structures with good accuracy.

The paper is organised as follows. We first introduce the large-eddy-simulation database used in the study. We then describe the analysis and modelling frameworks used. This is followed by a presentation of the results of the SPOD and linear stability analyses. The subsequent section presents the resolvent analysis, and the paper is completed with conclusions.

II. Numerical Database

We use a numerical database obtained from a high-fidelity large eddy simulation of a $M=0.4$ isothermal turbulent jet, using the compressible flow solver ‘Charles’ developed at Cascade Technologies.¹⁵ This database is an extension of the previous work by Brès *et al.*⁹ and validated for the same nozzle configuration at $M=0.9$. The Reynolds number based on mean jet exit velocity U_j and the nozzle diameter D is, $Re_D = U_j D / \nu \approx 4.5 \cdot 10^5$. The cylindrical coordinate system is centered at the jet exit $(0,0,0)$ in the computational domain that extends from $-10D$ to $50D$ in the streamwise direction and spreads from $20D$ to $50D$ in the radial direction.

Wall modelling and near-wall adaptive mesh refinement are employed on the internal nozzle surface.⁹ The near-wall resolution was chosen based on an initial estimate of the experimental nozzle-exit boundary-layer thickness, to yield approximately 10-20 LES cells in the developing boundary layer region. The resulting wall-normal grid spacing in wall units y_{LES}^+ is of order $O(70)$, and of order $O(100)$ for the streamwise and azimuthal grid spacings for the present case. Therefore, the physics of the viscous sublayer is modelled with wall modelling, and the results in the (very) near-wall region should be considered with caution. However, the bulk of boundary layer dynamics, and in particular the large-scale structures that are as large as the boundary layer thickness are well resolved and accurately captured in the LES.

Synthetic turbulence boundary conditions are used at $-2.8 < x/D < -2.5$ on the internal nozzle surface, in order to replicate the boundary layer trip in the companion experiment;⁹ this leads to turbulent boundary-layer profiles at the nozzle exit, in close agreement with the experimental results of Cavalieri *et al.*⁴ An upstream position $x/D = -2.8$ bounds the streamwise extent of the available nozzle data upstream of the jet exit plane. The total simulation time is $t_{sim} = t_{sim}^* c_\infty^* / D = 2000$ and the sampling period of the flow field is $\Delta t = \Delta t^* c_\infty^* / D = 0.2$. This provides 10000 snapshots. More details on the simulation are provided in Brès *et al.*⁹

III. Spectral analysis and modelling

A. Spectral Proper Orthogonal Decomposition (SPOD)

We employ SPOD to educe coherent structures from the NBL and in the downstream region of the turbulent jet. SPOD provides an orthogonal basis of modes that are ranked according to their energy at a given frequency. The basis provides an optimal compression in terms of the fluctuation energy with respect to a specified norm. We perform SPOD by following the recipe provided by Towne *et al.*,¹⁴ and in what

follows we briefly outline the procedure.

Since the jet is periodic in azimuth, we first decompose the fluctuation field $q(x, r, \theta, t)$, containing flow variables $q = [\rho, u_x, u_r, u_\theta, T]^T$, into its azimuthal components:

$$q(x, r, \theta, t) = \sum_{m=-\infty}^{m=\infty} \tilde{q}_m(x, r, t) e^{-im\theta} \quad (1)$$

where m is azimuthal mode number and \tilde{q}_m the associated modal amplitude. An assumption of ergodicity enables consideration of different temporal segments of the signal as statistically independent realisations of the jet. The time signal is partitioned into the 50% overlapping segments containing 256 snapshots, providing $N_b = 78$ independent ensembles of the jet fluctuations. Then short-time Fourier transforms are applied to the segments of time series to obtain the temporal Fourier modes $\hat{q}_{m\omega}$. The current study is solely concerned with the axisymmetric component ($m = 0$) of the flow field, hence we drop the m in what follows.

To perform SPOD, Fourier realisations are first stored in a matrix Q_ω for each frequency:

$$Q_\omega = [\hat{q}_\omega^{(1)} \hat{q}_\omega^{(2)} \hat{q}_\omega^{(3)} \dots \hat{q}_\omega^{(n_{blocks})}] \quad (2)$$

A global cross-spectral-density matrix \mathbf{S}_ω for given frequency is calculated as

$$\mathbf{S}_\omega = Q_\omega Q_\omega' \quad (3)$$

Finally, SPOD modes are obtained through eigendecomposition of the weighted cross-spectral-density matrix:

$$\mathbf{S}_\omega \mathbf{W} = \mathbf{\Psi}_\omega \mathbf{\Lambda}_\omega \mathbf{\Psi}_\omega^{-1} \quad (4)$$

Here, $\mathbf{\Psi}_\omega$ is the set of SPOD modes for angular frequency, ω and its i^{th} column is the i^{th} SPOD mode ψ^i . The energies of the modes are contained in the diagonal eigenvalue matrix $\mathbf{\Lambda}_\omega = \text{diag}(\lambda^1, \lambda^2, \dots, \lambda^{n_{blocks}})$. \mathbf{W} is the weight matrix associated with the numerical integration and compressible energy norm¹⁶ applied in the computation. SPOD modes satisfy the orthogonality relation under this weight, i.e:

$$\langle \psi^i, \psi^j \rangle_{\mathbf{W}} = \delta_{ij} \quad (5)$$

B. Local linear spatial stability analysis of nozzle flow

Models based on linear theory have been used extensively to model wavepackets in turbulent jets. In these models, the linearised Navier Stokes equations are computed using the turbulent mean flow as a base flow. We implement such a modelling strategy in the nozzle.

In this paper we choose to use a simplified stability model, based on a two-dimensional, locally parallel, incompressible base flow. Under the assumption that mean flow is homogeneous in the streamwise direction x and in time t , wave-like perturbations take the form:

$$\tilde{q}(x, y, t) = \hat{q}(y) e^{i(\alpha x - \omega t)} \quad (6)$$

where $q = [u, v, p]^T$ is the vector of flow variables; streamwise and wall-normal velocities, and pressure. Substituting the perturbation ansatz into the incompressible Navier Stokes equations and linearising around the mean flow recasts the equations as generalised eigenvalue problem $\mathbf{L}\hat{q} = \alpha\mathbf{F}\hat{q}$, whose solution for given a Reynolds number Re and angular frequency ω yields eigenvectors $\hat{q} = [\hat{u} \ \hat{v} \ \hat{p}]^T$ with corresponding eigenvalues α :

$$\begin{bmatrix} \omega - \frac{D^2}{Re} i & U' & 0 \\ 0 & \omega - \frac{D^2}{Re} i & iD \\ 0 & iD & 0 \end{bmatrix} \begin{bmatrix} \hat{u} \\ \hat{v} \\ \hat{p} \end{bmatrix} = \alpha \begin{bmatrix} U & 0 & 1 \\ 0 & U & 0 \\ I & 0 & 0 \end{bmatrix} \begin{bmatrix} \hat{u} \\ \hat{v} \\ \hat{p} \end{bmatrix} \quad (7)$$

where α refers to the streamwise wavenumber. Due to the high Reynolds number of the flow, α^2 viscous terms are neglected, similarly to what was done by Rodriguez *et al.*¹⁷ For a specified Re number and ω , spatial growth or decay is governed by the imaginary part of the wavenumber: if $\alpha_i < 0$ the disturbance will experience a growth in the positive x direction.

Chebyshev polynomials are used to discretise the domain, with a numerical grid spanning $y = [-1, 1]$. 601 Chebyshev collocation points were found to be sufficient for convergence of the free-stream and boundary-layer branches of the spectrum.

The above equations are completed with Dirichlet boundary conditions

$$\hat{u} = \hat{v} = 0 \text{ at } y = 1 \text{ and } y = -1. \quad (8)$$

We use the displacement thickness of the boundary-layer δ_1 and mean centreline velocity U_{x_0} at a streamwise position x_0 as the characteristic length and velocity scales respectively, thus setting the Reynolds number as $Re = U_{x_0} \delta_1 / \nu = Re_{\delta_1}$ in the local stability analysis. With this Reynolds number as an input, we use the velocity function proposed by Monkewitz *et al.*¹⁸ for zero pressure gradient turbulent boundary layer flows to fit the LES flow. In a compact form, the expression can be written as

$$U = f(y^+, Re) \quad (9)$$

where $y^+ = u_\tau y / \nu$ stands for dimensionless wall-normal distance in inner (viscous) units. The friction velocity u_τ is computed through the analytical function proposed by Österlund *et al.*¹⁹ as

$$u_\tau = \left[\frac{1}{\kappa} \ln(Re_{\delta_2}) + C \right]^{-1} \quad (10)$$

where Re_{δ_2} is the Reynolds number based on local momentum thickness, $\kappa = 0.41$ and $C = 5.1$. The analytical formulation leads to velocity profiles with well-behaved and smooth derivatives throughout the domain. Explicit expression of the velocity function can be found in Cossu *et al.*²⁰ A comparison between computed fit and the mean nozzle flow is shown in Figure 1.

The scalings of velocity and angular frequency in the analysis can be recast in terms of above non-dimensionalisation parameters as

$$\omega = 2\pi St \delta_1^{x_0} \quad (11)$$

$$U = \frac{U_{LES}}{U_{LES}^{x_0}}. \quad (12)$$

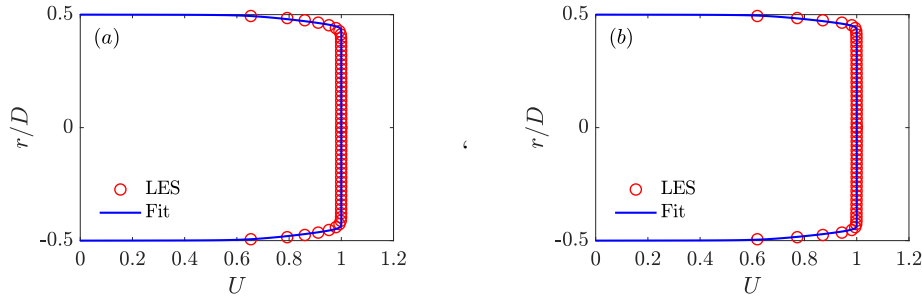


Figure 1: Radial profiles of the nozzle mean flow and analytic fit at (a) $x_0 = x/D = -1$ and (b) $x_0 = x/D = -1.5$.

C. Modal decomposition of LES data

The LST eigenbasis is used to expand the leading SPOD mode as

$$\hat{\mathbf{q}}_{POD}^{x_0}(r) = \sum_n a_n \hat{q}^{x_0}(r) \quad (13)$$

where a_n is the complex amplitude of the stability eigenfunction, $\hat{q}^{x_0}(r)$. which is a complex-valued coefficient. The amplitudes, a_n are obtained by projection of the leading SPOD mode onto sets of linear modes. We follow the orthogonal projection methodology used by Passagia *et al.*²¹ This consists in, for each frequency, orthonormalization of the non-orthogonal linear basis through a Gram-Schmidt procedure,

projecting the data onto the orthonormal basis and obtaining corresponding amplitudes, and recovering the true amplitudes of the non-normal linear modes. The procedure is detailed in Alizard *et al.*²²

The number of linear modes required to characterise the leading SPOD mode is a central question to the analysis. We use different numbers of eigenmodes in the basis to make the projection, starting with single mode representation, followed by all of the boundary-layer modes, and finally adding modes from the free-stream branch. We denote these, respectively, as rank-1, ‘Rank-BLB’ and ‘Rank-BLB+FS’ truncations of the eigenbasis.

D. Resolvent analysis of nozzle flow

In locally parallel resolvent analysis, the system of incompressible Navier-Stokes equations are arranged in matrix form

$$\left(-i\omega \begin{bmatrix} I & 0 & 0 \\ 0 & I & 0 \\ 0 & 0 & I \end{bmatrix} + \begin{bmatrix} \alpha i U - \frac{\alpha^2 - D^2}{Re} i & U' & \alpha i \\ 0 & \alpha i U - \frac{\alpha^2 - D^2}{Re} i & D \\ \alpha i & D & 0 \end{bmatrix} \right) \begin{bmatrix} \hat{u} \\ \hat{v} \\ \hat{p} \end{bmatrix} = \begin{bmatrix} \hat{f}_x \\ \hat{f}_y \\ \hat{0} \end{bmatrix} \quad (14)$$

where \hat{f}_x and \hat{f}_y denote momentum forcing. The notation introduced in linear stability analysis is maintained. We furthermore introduce matrices \mathbf{B} and \mathbf{C} , which allows us to consider forcing only through momentum equations and that the associated response/output $\hat{\mathbf{y}}$ comprise solely velocity fluctuations, representing turbulent kinetic energy. The input-output system can be written in compact form as

$$\mathbf{L}\hat{\mathbf{q}} = \mathbf{B}\hat{\mathbf{f}} \quad (15)$$

$$\mathbf{C}\hat{\mathbf{q}} = \hat{\mathbf{y}} \quad (16)$$

where \mathbf{L} is the linearised incompressible Navier-stokes operator, and $\hat{\mathbf{f}}$ stands for the unknown input/forcing. The matrices \mathbf{B} and \mathbf{C} are defined as

$$\mathbf{B} = \begin{bmatrix} I & 0 \\ 0 & I \\ 0 & 0 \end{bmatrix} \text{ and } \mathbf{C} = \mathbf{B}^T. \quad (17)$$

The relation between input and output can be established by introducing the resolvent operator \mathbf{R} as

$$\hat{\mathbf{y}} = \mathbf{C}\mathbf{L}^{-1}\mathbf{B}\hat{\mathbf{f}} = \mathbf{R}\hat{\mathbf{f}}. \quad (18)$$

The aim of the resolvent analysis is to obtain a forcing that maximise the norm of the associated response. This can be formulated via the Rayleigh quotient

$$G_{max}^2(\hat{f}) = \max \frac{\langle \hat{\mathbf{y}}, \hat{\mathbf{y}} \rangle_{\mathbf{W}_y}}{\langle \hat{\mathbf{f}}, \hat{\mathbf{f}} \rangle_{\mathbf{W}_f}} = \frac{\|\mathbf{R}\hat{\mathbf{f}}\|_{\mathbf{W}_y}^2}{\|\hat{\mathbf{f}}\|_{\mathbf{W}_f}^2} \quad (19)$$

where $\|\cdot\|_{\mathbf{W}}$ stands for the Euclidian norm under the induced weight \mathbf{W} , which is a positive Hermitian matrix and is here identical for input and output spaces. Singular value decomposition of the weighted resolvent operator allows to obtain forcing-response modes that maximise the Rayleigh quotient

$$\mathbf{W}^{1/2}\mathbf{R}\mathbf{W}^{-1/2} = \mathbf{U}\mathbf{\Sigma}\mathbf{V}^* \quad (20)$$

where $*$ denotes the conjugate transpose, $\mathbf{W}^{1/2}$ is computed through Cholesky decomposition of the weight matrix $\mathbf{W} = \mathbf{W}^{1/2}\mathbf{W}^{1/2*}$, $\mathbf{U} = [U^{(1)}, U^{(2)}, \dots, U^{(N)}]$ and $\mathbf{V} = [V^{(1)}, V^{(2)}, \dots, V^{(N)}]$ are the left and right singular vectors, and $\mathbf{\Sigma}$ is a diagonal matrix containing singular values $\mathbf{\Sigma} = \text{diag}(\sigma_1, \sigma_2, \dots, \sigma_N)$ in decreasing order.

Equation (20) can be rearranged to define forcing and response bases in terms of left and right singular vectors of the modified resolvent operator as

$$\Psi^{(i)} = \mathbf{W}^{-1/2} U^{(i)} \quad (21)$$

$$\Phi^{(i)} = \mathbf{W}^{-1/2} V^{(i)}. \quad (22)$$

The response and forcing modes are orthonormal in their respective space

$$\langle \Psi^{(i)}, \Psi^{(j)} \rangle_W = \langle \Phi^{(i)}, \Phi^{(j)} \rangle_W = \delta_{ij}. \quad (23)$$

Equation (18), together with the newly introduced variables, can be rewritten into following final form:

$$\hat{\mathbf{y}} = \mathbf{R} \hat{\mathbf{f}} = \Psi \Sigma \Phi^* \mathbf{W} \hat{\mathbf{f}} \quad (24)$$

which shows that if a forcing $\hat{\mathbf{f}} = \phi^{(1)}$ is applied, the output is response mode amplified by the first singular value, i.e. $\hat{\mathbf{y}} = \sigma_1 \psi^{(1)}$. Thus we denote this forcing-response pair as optimal resolvent mode. The singular value, σ_1 , indicates the gain associated with the optimal forcing-response mode pair.

To employ the resolvent analysis, the computational domain, considered in the preceding linear stability analysis, is discretised using 401 Chebyshev collocation points. Dirichlet boundary conditions are employed for two velocity components at the wall, and the governing equations are similarly non-dimensionalised with the local displacement thickness and mean centerline velocity.

IV. Results

A. Coherent structures in the nozzle

In this section we present the results of SPOD analysis of turbulent jet. The weight matrix \mathbf{W} in equation (4) allows the calculation of POD modes that optimally describe flow dynamics in specified region. Two choices are considered. We first attribute zero weight to the nozzle region, and seek modes that maximise the energy downstream of the jet exit. We denote these as ‘Jet-Weighted’ SPOD modes. Subsequently, we exclude the jet region to identify energy maximising modes in the nozzle, i.e. ‘Nozzle-Weighted’ SPOD modes.

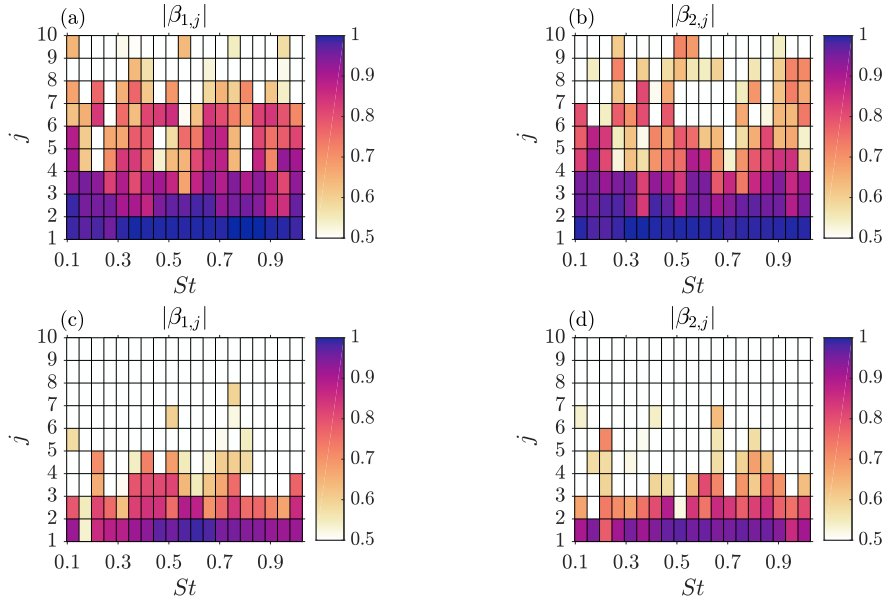


Figure 2: Convergence maps for ‘Nozzle-Weighted’ (top row) and ‘Jet-Weighted’ (bottom row) SPOD analyses.

In addition to the SPOD analysis with the full data, we perform a convergence study by splitting the data into two subsets each containing half the number of available independent realisations. To assess convergence, we then compute normalised inner product $\beta_{i,j}$ between each SPOD mode ψ_j of the full set and $\psi_{i,j}$ of subsets:

$$\beta_{i,j} = \frac{\langle \psi_{i,j}, \psi_j \rangle}{\|\psi_{i,j}\|_W \|\psi_j\|_W} \text{ for } St = 0.1, 0.2, \dots, 1 \quad (25)$$

where the variables corresponding to each subset are denoted by i . Correlation coefficient β acquires values between 0 and 1, where $\beta = 1$ for a given SPOD mode indicates a satisfactory convergence, i.e the SPOD mode preserves its shape with increasing number of realisations.^{23,24}

Figure 2 shows the correlation map obtained for varying frequencies. It demonstrates that both ‘Jet-Weighted’ and ‘Nozzle-Weighted’ SPOD analyses are reasonably converged as far as the leading modes are concerned, providing values of β larger than 0.8. In ‘Nozzle-Weighted’ SPOD, the level of agreement is preserved for the first two sub-optimal modes for most of the frequencies, whereas in ‘Jet-Weighted’ SPOD, the correlation is around 0.6-0.7 for first suboptimal modes, and drops abruptly to low levels for higher-order modes. The results altogether indicate that both SPOD analyses provide converged leading modes; it is these that are considered in the analysis throughout the paper.

Figure 3 shows the leading ‘Jet-Weighted’ SPOD mode of streamwise velocity ($m = 0$) for different frequencies. Wavepackets are clearly present both in the NBL and the jet, indicating a coupling between these two regions. Similar boundary-layer structures have been observed in a turbulent flow over an airfoil by Abreu *et al.*²³ Reliable detection of structures proves to be difficult at low frequencies (e.g. $St = 0.2$), for which wavelengths exceed the length of the nozzle domain.

We now wish to determine whether the nozzle structures shown to be connected to jet wavepackets via ‘Jet-Weighted’ SPOD are also the most energetic NBL structures. Figure 4 compares the velocity fields of the leading ‘Jet-Weighted’ and ‘Nozzle-Weighted’ SPOD within the nozzle. Note that ‘Jet-Weighted’ SPOD modes are taken from Figure 3. This comparison clearly shows high similarity between the two type of SPODs specifically for $St > 0.2$, suggesting that the leading SPOD modes within the nozzle, which are relevant to the downstream jet dynamics in terms of energy, are also the most-energetic nozzle structures.

In what follows, we consider linear stability theory (LST) to model the NBL structures deduced by ‘Nozzle-Weighted’ SPOD, as the modes obtained by this SPOD are better converged than those deduced by ‘Jet-Weighted’ SPOD. Hence the prefix ‘Nozzle-Weighted’ is dropped in the remainder of the paper. The analysis using ‘Jet-Weighted’ SPOD is not reported in the paper, but its results led to similar conclusions.

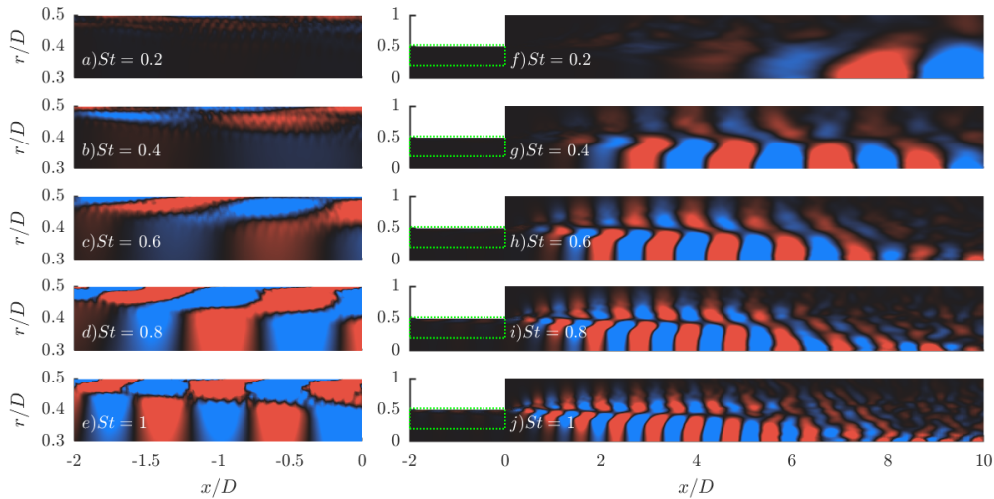


Figure 3: Leading ‘Jet-Weighted’ SPOD mode of streamwise velocity ($m = 0$) at varying frequencies (right column), saturated zoom-in on the nozzle (left column). The velocity field is normalised with its absolute value in the domain. Contour colours show negative (blue) and positive (red) values of the field (Colour map courtesy of Kovasi²⁵).

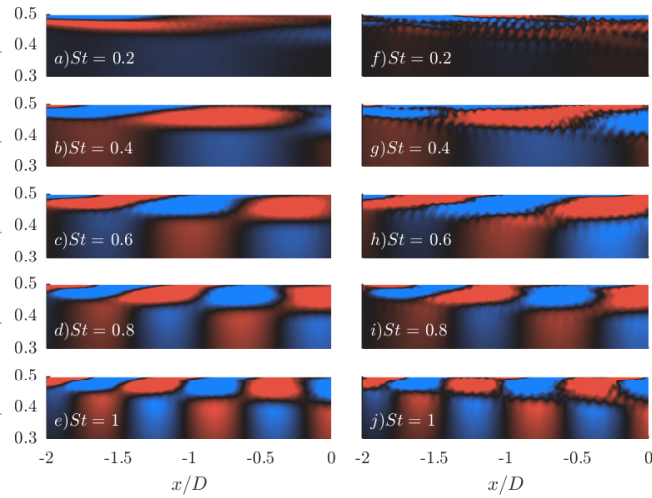


Figure 4: Leading ‘Nozzle-Weighted’ (left column) and ‘Jet-Weighted’ (right column) SPOD mode of streamwise velocity ($m = 0$) in the nozzle for different frequencies. Each velocity field is normalised with its absolute value in the nozzle. Phases of the ‘Jet-Weighted’ SPOD mode are shifted in order to make clear comparisons.

B. Local spatial stability analysis of the nozzle mean flow

We here consider the two-dimensional incompressible linearised Navier-Stokes equations as a simplified model for the educed NBL structures.

Figure 5 shows eigenspectra for varying St at streamwise position $x/D = -1.5$. These comprise two families of stable modes; free-stream modes, shown in blue, and boundary-layer modes, shown in red. Radial structure of eigenmodes from two branches is shown in Figure 6c. The 2D mean flow considered leads to symmetric and antisymmetric eigenmodes. Only the even modes are considered, as a surrogate for the axisymmetric modes of the NBL dynamics.

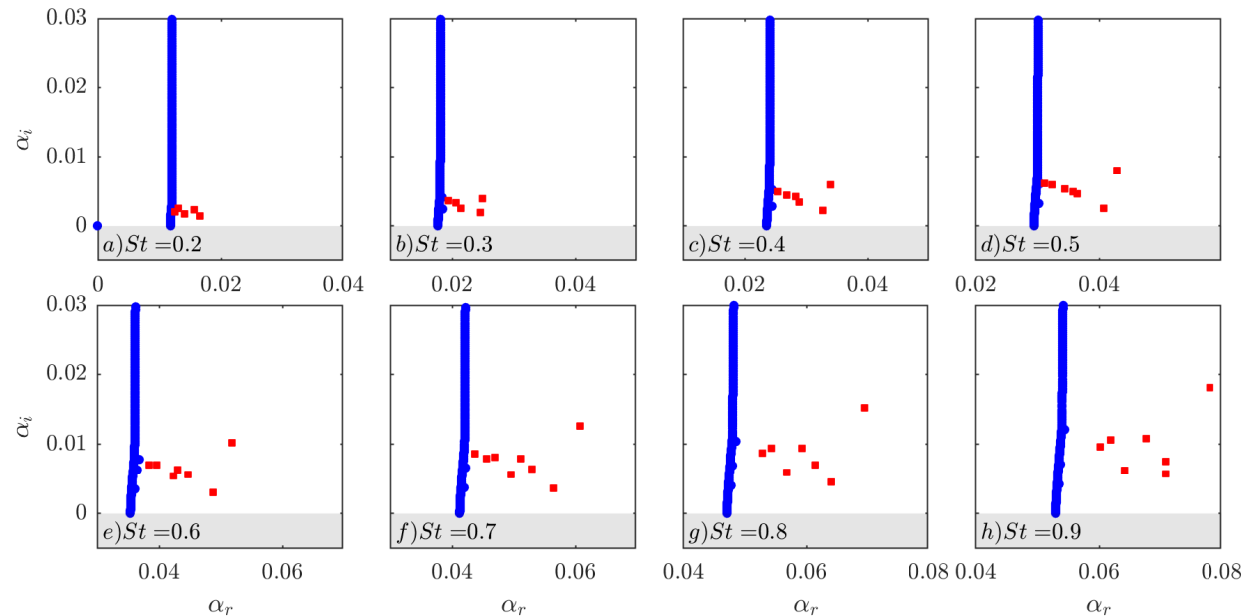


Figure 5: Eigenvalue spectrum at varying frequencies for $x_0 = x/D = -1.5$. (■) Boundary-layer modes; (●) Free-stream modes.

The structures observed in the SPOD analysis are confined within the NBL, suggesting that the boundary-layer eigenmode branch is appropriate for their description. To assess the agreement between educed struc-

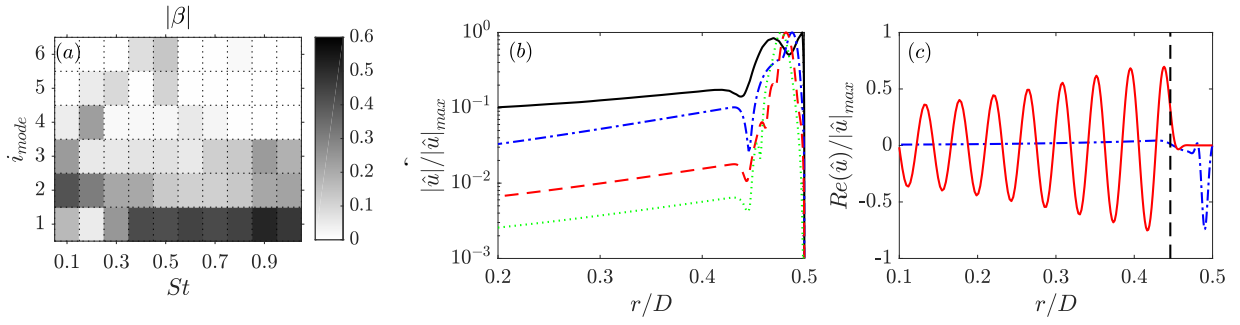


Figure 6: (a) Normalised scalar product between i^{th} discrete stability eigenmode and the leading SPOD mode at $x/D = -1.5$ (bottom to top row : least to most stable discrete modes). Normalised streamwise velocity profiles for $St = 0.6$: (b) Leading SPOD mode (black solid line); Discrete modes: Least-stable (blue dash-dot line); 2nd least-stable (red dashed line); 3rd least-stable (green dot line). Corresponding eigenvalues are shown in Figure 5e. (c) An eigenmode from free-stream branch (solid red lines) and boundary-layer branch (blue dash-dot line). Local boundary layer thickness (black dashed line).

tures and stability eigenmodes, we again define a similarity metric β , which is normalised inner product between discrete mode q_i and the leading SPOD mode q_{pod} . The eigenmodes are ranked according to their decay rate, with $i = 1$ the least-stable mode. The inner product and β are defined, respectively, as

$$\langle x(r), y(r) \rangle = \int_0^r x(r)y^*(r)rdr \quad (26)$$

$$\beta_i(St) = \frac{\langle \hat{q}_i^{x_0}, \hat{q}_{POD}^{x_0} \rangle}{\|\hat{q}_i^{x_0}\| \cdot \|\hat{q}_{POD}^{x_0}\|}. \quad (27)$$

Figure 6a presents the correlation map obtained, showing a close agreement between certain of the LST modes, particularly least stable modes (bottom row), and the data over a range of frequencies. Comparison between the data and the first three least-stable modes, shown in (Figure 6b), shows how these have qualitatively similar structures. This is a first indication that LST may be a useful tool for description of the NBL structures shown earlier to be linked to jet wavepackets. In what follows, we aim to represent nozzle dynamics in terms of eigenmodes via projections.

C. Modal decomposition of the nozzle data

In this section, we reconstruct the leading SPOD mode of streamwise velocity using varying numbers of eigenmodes. The radial structure of the leading SPOD mode, can be written as a summation of eigenmodes as

$$\hat{\mathbf{q}}_{POD}^{x_0}(r) = \sum_n a_n \hat{q}^{x_0}(r). \quad (28)$$

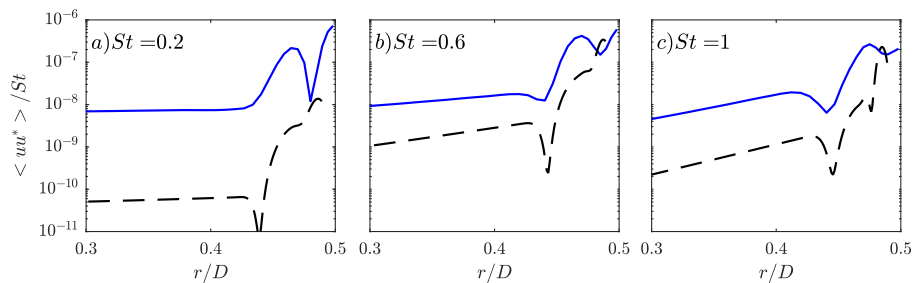


Figure 7: Radial profiles of the streamwise velocity ($m = 0$) at $x_0 = -1.5$. The leading SPOD mode (blue solid lines) and rank-1 stability model (black dashed lines).

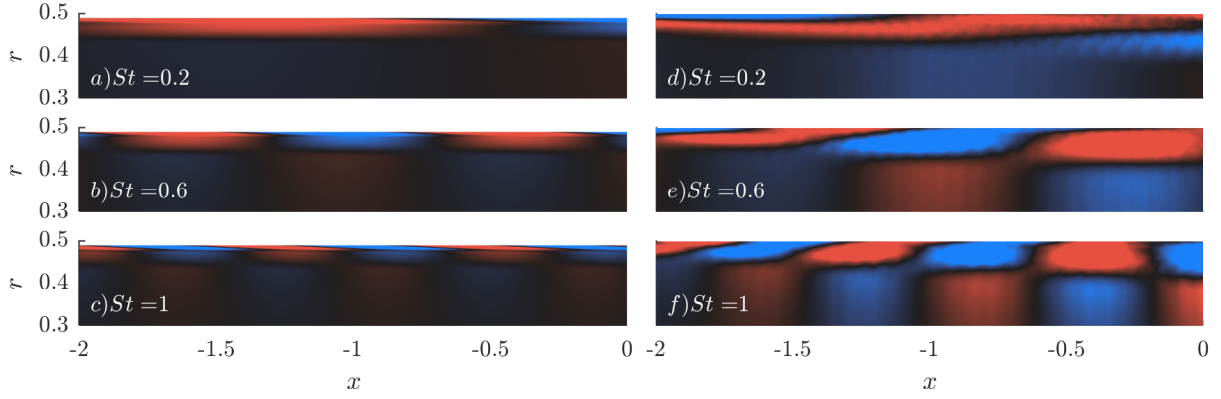


Figure 8: Real component of the streamwise velocity ($m = 0$). Left: Rank-1 stability model; Right: Leading SPOD mode.

We perform projections of the leading SPOD mode onto three truncated eigenbases of different rank to compute the modal amplitudes at $x_0 = x/D = -1.5$, as outlined in Section IIIC.

A rank-one description of the SPOD modes is first evaluated, by projecting on the least-stable mode of the boundary layer branch. We select three representative frequencies $St = 0.2, 0.6, 1$ to present the results. It can be seen in Figure 7 that single-mode representation provides a poor description of the data.

For a given frequency, we can reconstruct a perturbation field in terms of linear modes as

$$\tilde{q}(x, r) = \sum_n a_n \hat{q}^{x_0}(r) e^{i\alpha_n(x-x_0)}. \quad (29)$$

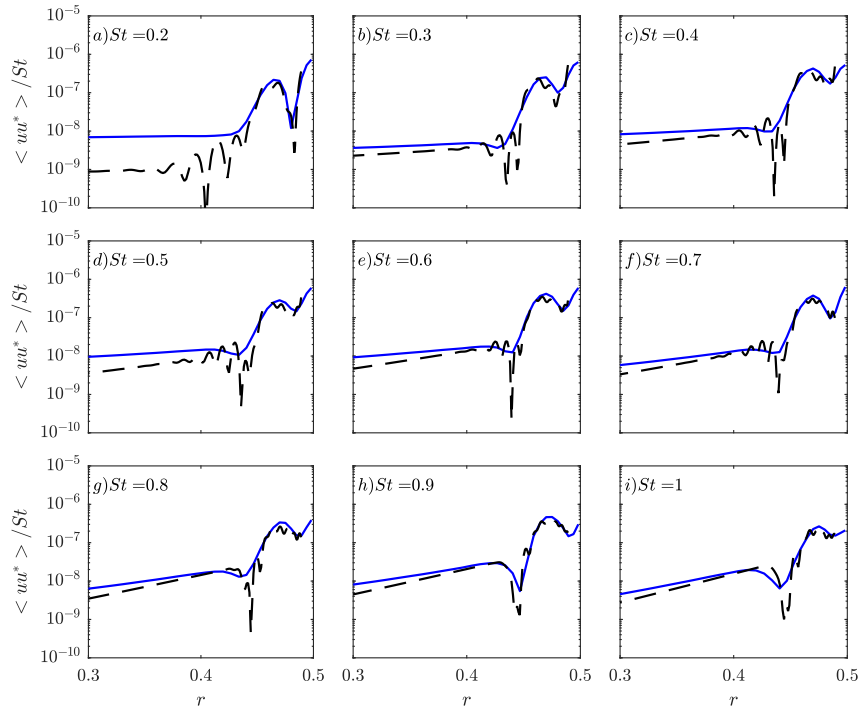


Figure 9: Radial profiles of the streamwise velocity ($m = 0$) at $x/D = -1.5$. The leading SPOD mode (blue solid lines) and ‘Rank-BLB’ stability model (black dashed lines). Note that the number of the eigenmodes N in the projection varies across frequencies. $N_{min} = 5$ for $St = 0.1$ and $N_{max} = 8$ for $St = 0.7$.

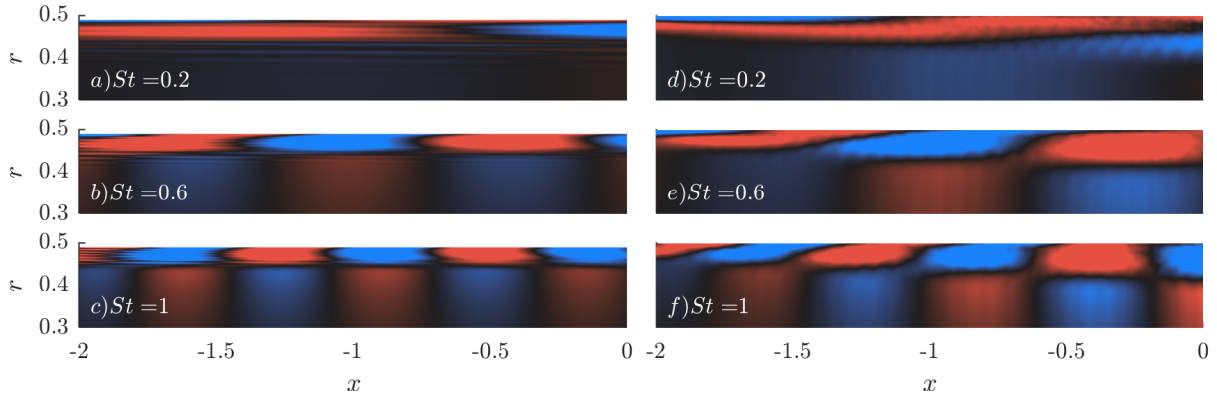


Figure 10: Real component of the streamwise velocity ($m = 0$). Left: ‘Rank-BLB’ stability model; Right: The leading SPOD mode.

We compare this field with the leading SPOD mode within the nozzle. Figure 8 shows, consistent with the poor agreement in radial structure shown in Figure 7, that a single-mode reconstruction agrees poorly with the data for all the frequencies considered. Single mode expansions using other modes of the boundary layer branch lead to similarly poor agreement, suggesting that a superposition of eigenmodes may be necessary.

A second low-rank description is obtained by projection on the eigenmodes of the boundary layer branch (‘Rank-BLB’). Agreement with the leading SPOD mode is now considerably improved, as shown in Figure 9. The comparisons of the spatial reconstruction for three representative frequencies clearly show substantial agreement with the leading SPOD modes (Figure 10).

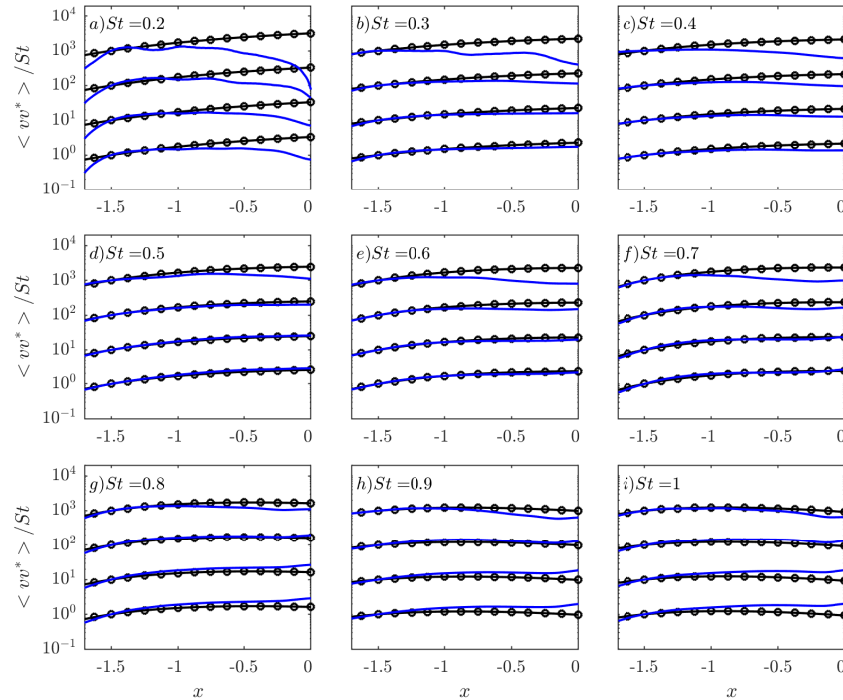


Figure 11: The normalised PSD envelopes of wall-normal velocity at several radial positions: The leading SPOD mode (blue solid line), ‘Rank-BLB’ stability model (black dotted line). From bottom to top: $r = 0.38, 0.4, 0.42, 0.44$. The curves are shifted by factor of 10 with increasing r .

This suggests that the NBL structures educed using SPOD are underpinned by non-modal dynamics.

Non-modal dynamics have been found to be important for wavepackets towards the end of potential core in turbulent jets, where streamwise evolution of wavepackets is underpinned by the Orr mechanism.²⁶ The Orr mechanism is also known to be responsible for non-modal growth of perturbations in the logarithmic layer of turbulent boundary layers.²⁷ Its characteristic signature is cycle of amplification followed by decay of the wall-normal/radial velocity fluctuations, and with an associated tilting of structures into the mean flow direction.

We therefore compare the SPOD mode and ‘*Rank-BLB*’ reconstructed wavepacket in terms of the streamwise evolution of wall-normal velocity. The comparison is shown in Figure 11: PSD of wall-normal velocity at several radial positions $r/D > 0.38$ are shown. Globally, the evolution of the wall-normal velocity fluctuations, which exhibits growth and decay consistent with the Orr mechanism, is captured by the reconstruction using boundary-layer modes.

Finally, we include free-stream modes in the projection (‘*Rank-BLB+FS*’). With the contribution of these modes (Figure 12 and 13), the agreement is further improved, as should be expected given that projection with the entire eigenbasis, which is complete, should result in an exact description of the data. However, comparison of the ‘*Rank-BLB*’ and ‘*Rank-BLB+FS*’ reconstructions shows how the essential details of the NBL structures have been captured by the former. This confirms that the coherent boundary layer structures, shown earlier to be connected to wavepackets in the jet, may be described with a low-rank, non-modal, stability model. It is therefore appropriate to place further analysis in a resolvent framework.

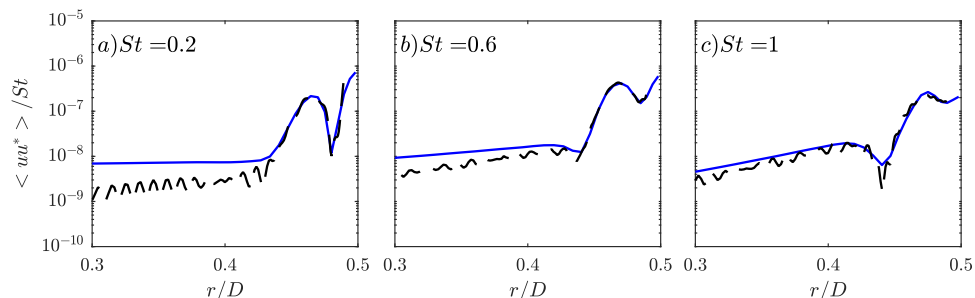


Figure 12: Radial profiles of the streamwise velocity ($m = 0$) at $x/D = -1.5$. The leading SPOD mode (blue solid lines) and ‘*Rank-BLB+FS*’ stability model (black dashed lines). Eigenmodes from free-stream branch ($M = 90$) and all the boundary-layer modes are included in the projection.

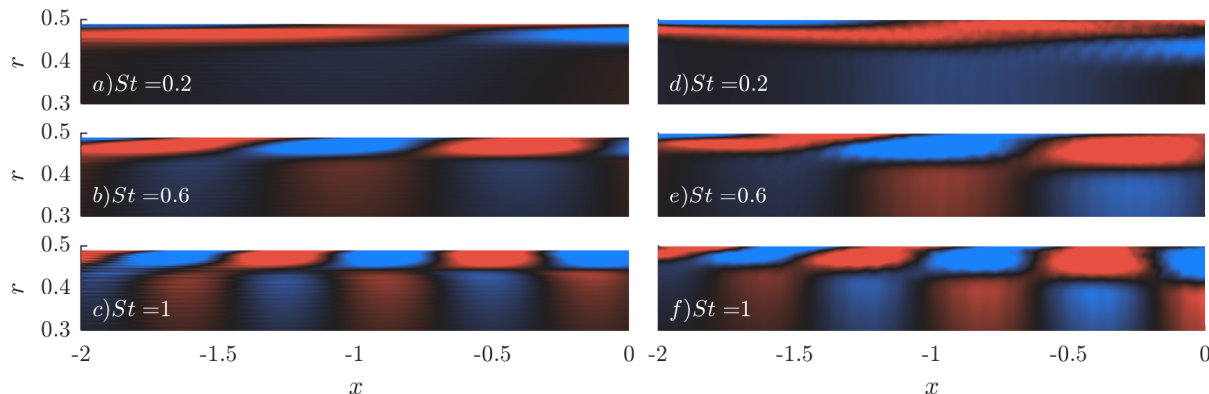


Figure 13: Real component of the streamwise velocity ($m = 0$). Left: ‘*Rank-BLB+FS*’ stability model; Right: The leading SPOD mode.

D. Local resolvent analysis of the nozzle mean flow

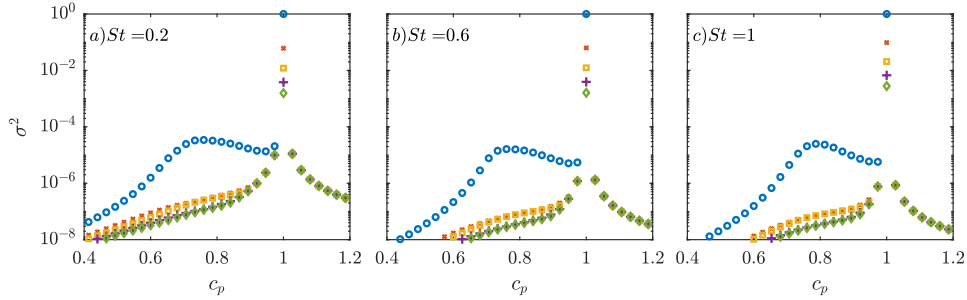


Figure 14: Resolvent gain curves as a function of disturbance phase speed c_p at varying frequencies for $x/D = -1.5$: (○) 1st Optimal mode; (×, □, +, ◇) Suboptimal modes in sequential order. Gains are normalised by maximum gain at each frequency.

The resolvent framework is appropriate for the description of coherent structures in systems whose eigenvalues are all stable. The dynamics are interpreted as being underpinned by external forcing that activates non-modal mechanisms such as identified in the previous section. The external forcing may be associated with ambient noise, non-linear wave interactions, or background turbulence. We here perform a resolvent analysis of the turbulent mean flow within the nozzle. The framework is, again, 2D, locally parallel and incompressible. Singular value decomposition of the resolvent operator provides orthonormal forcing and response bases ranked according to a set of gains obtained as the singular values of the resolvent operator.

The local resolvent formulation requires an angular frequency - wavenumber pair, $\omega - \alpha$, to be specified. We first consider a set of wavenumbers associated with phase speed c_p varying between 0.4 and 1.2 U_j . Figure 14 shows the gains as function of phase speed for a selection of the frequencies considered earlier. The gain curves show large peaks for disturbances with phase speed equal to the local mean jet-centerline velocity. This is associated with the possibility of generating large vortices in the extended free-stream region. These can achieve large fluctuation energy, simply on account of the large extent of the free-stream and the fact that such large vortices, feeling a higher effective Reynolds number, will be less damped by viscosity. These peaks are thus an artefact that we are not interested in, and that could be removed by the introduction of weights that would localise the resolvent analysis within the confines of the boundary layer. We also see that there is a significant gain separation between the optimal and sub-optimal modes. Finally, a broader peak is observed in the vicinity of $c_p = 0.7$. The resolvent modes in this range are those of interest, as they correspond to activity within the boundary layer. These findings are similar to the observations by Abreu *et al.*²³ in the resolvent analysis of the turbulent boundary layer over an airfoil.

Figure 15 shows how the phase speed of perturbations described by the leading SPOD mode have phase speed that varies across the boundary layer. This suggests a description in terms of multiple resolvent modes.

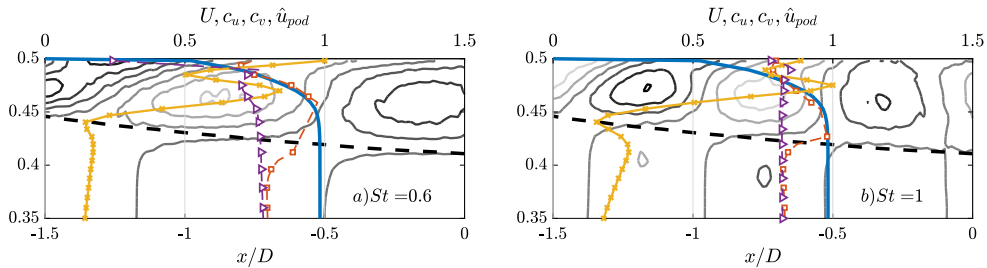


Figure 15: Contour plots: Real part of streamwise velocity of the leading SPOD mode ($m = 0$). Radial profiles pertinent to this mode at streamwise position $x/D = -1.5$: Phase speed of streamwise velocity (orange square-dashed lines); phase speed of radial velocity (purple triangle-dashed lines); normalised amplitude of streamwise velocity (yellow cross-solid lines). Nozzle mean flow (blue solid lines).

We first compare the leading SPOD and resolvent response modes for phase speed associated with the largest gain. Note that this phase speed roughly corresponds to the value associated with the wall-normal

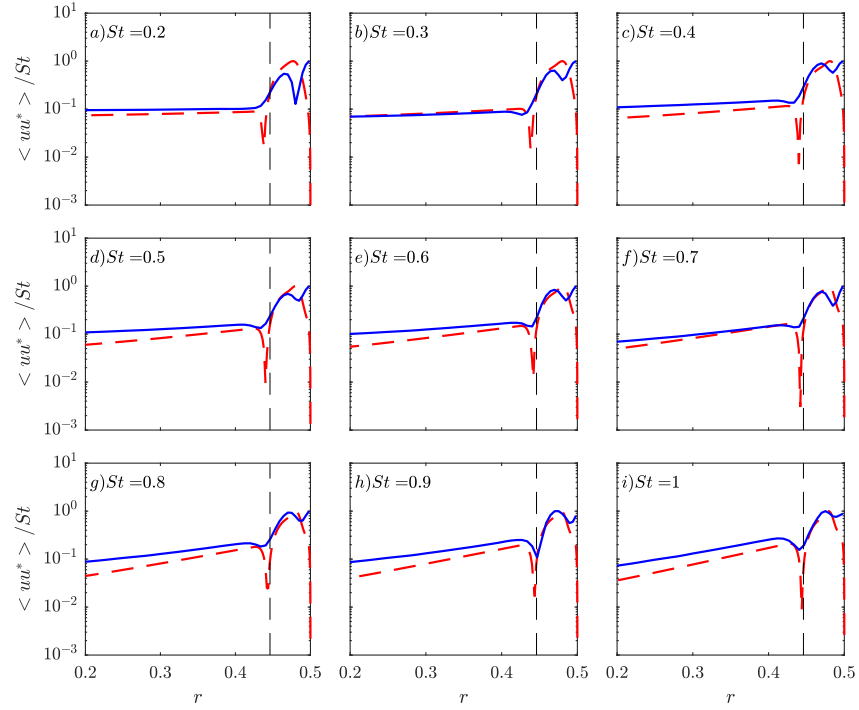


Figure 16: Radial profiles of normalised streamwise velocity ($m = 0$) at $x/D = -1.5$: The leading SPOD mode (blue solid lines) and optimal resolvent response mode (red dashed lines).

velocity of the SPOD mode. Figure 16 and 17 show good agreement over a wide range of frequencies.

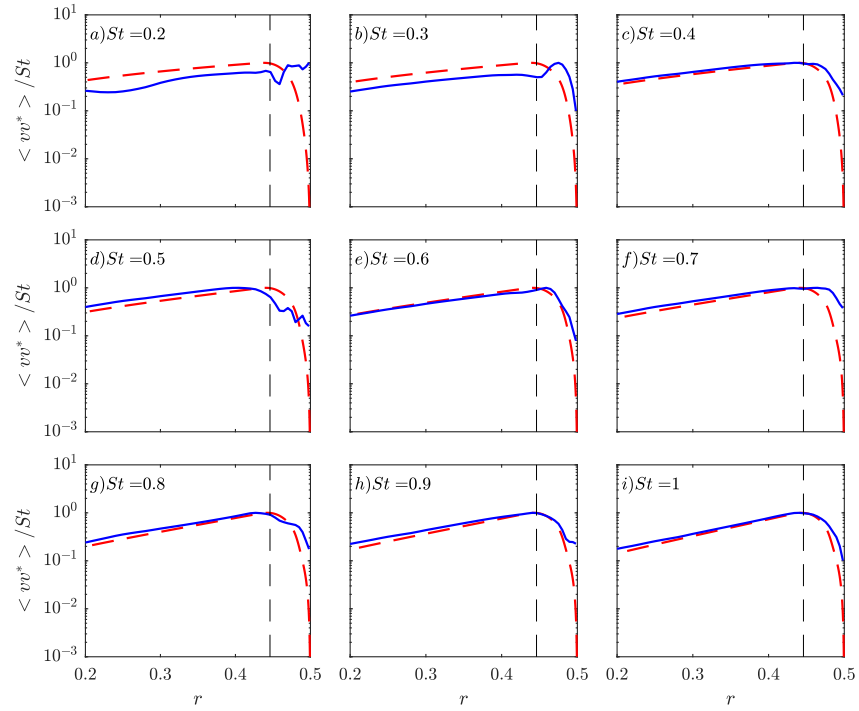


Figure 17: Radial profiles of normalised wall-normal velocity ($m = 0$) at $x/D = -1.5$: The leading SPOD mode (blue solid lines) and optimal resolvent response mode (red dashed lines).

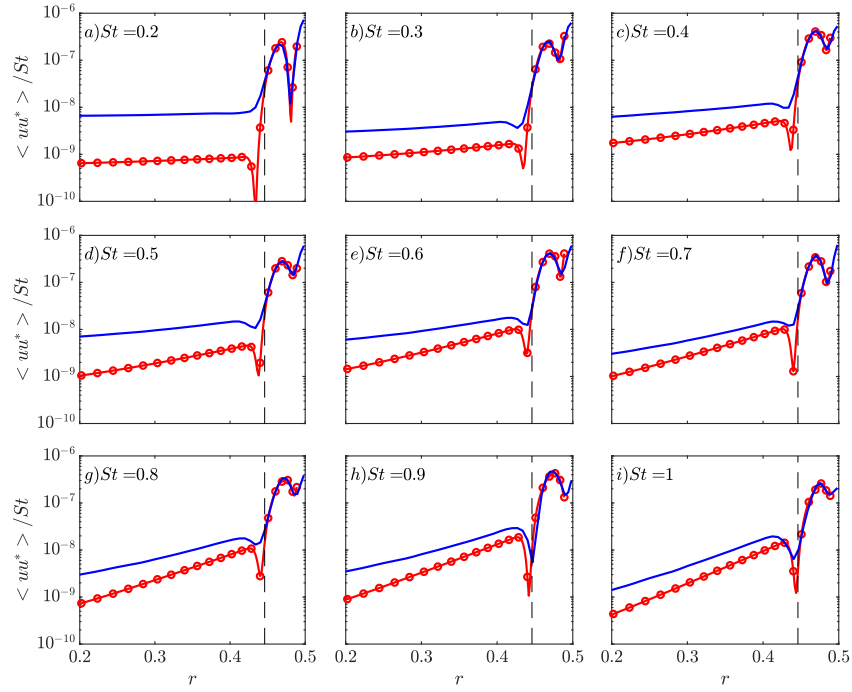


Figure 18: Radial profiles of streamwise velocity ($m = 0$) at $x/D = -1.5$: The leading SPOD mode (blue solid lines) and rank-4 resolvent model (red dotted lines).

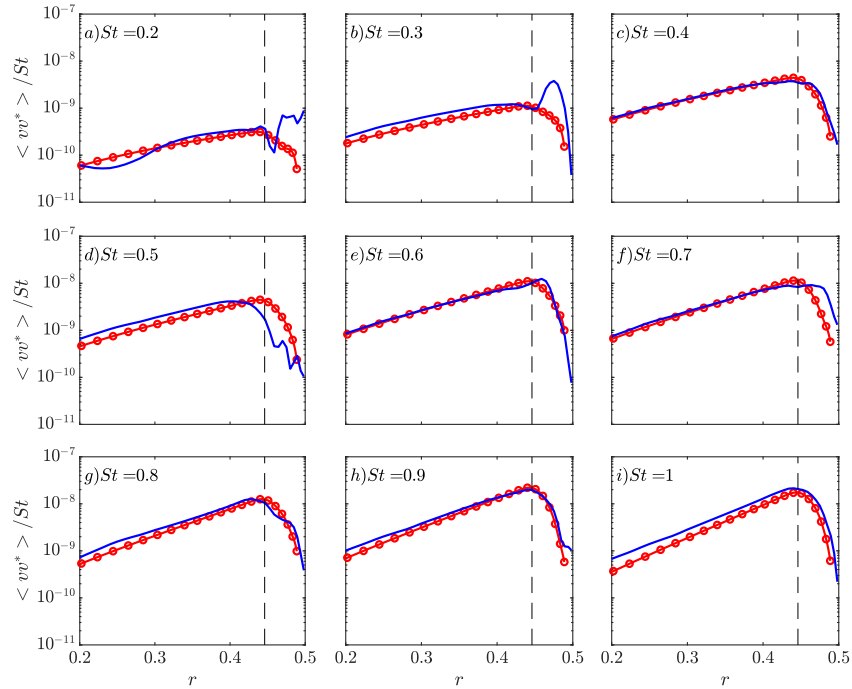


Figure 19: Radial profiles of wall-normal velocity ($m = 0$) at $x/D = -1.5$: The leading SPOD mode (blue solid lines) and rank-4 resolvent model (red dotted lines).

We then employ projection of the leading SPOD mode on a rank-4 basis comprised of optimal response modes with varying phase speeds. Informed from Figure 15, we include modes with phase speed equal to

0.7, 0.75, 0.8 and 0.85, and the comparisons are shown in Figure 18 and 19. Globally, the rank-4 resolvent model captures the local traits of the most energetic nozzle structures. Moreover, spatial reconstruction of a perturbation field compares favorably with the data, in which the structures tilt into the mean flow direction (Figure 20).

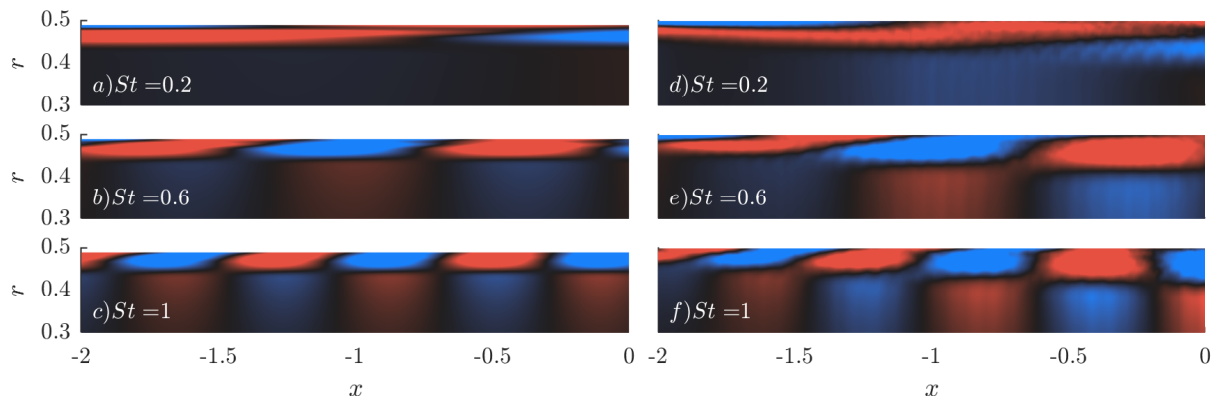


Figure 20: Real component of the streamwise velocity ($m = 0$). Left: Rank-4 resolvent model; Right: The leading SPOD mode.

Finally, optimal forcing fields are reconstructed in Figure 21, where a tilting of the forcing modes against the mean shear, characteristic of the Orr mechanism, is evident. Similar tilted organisation of forcing modes have been reported downstream of the jet exit in a local resolvent analysis of the same turbulent jet by Tissot *et al.*²⁶ Taken together with the results of the LST analysis, the present resolvent analysis suggests that the coherent nozzle structures pertinent to downstream jet dynamics can be considered as optimal linear modes in response to forcing modes tilted against the mean-shear, that exploits the non-linearities in the turbulent flow.

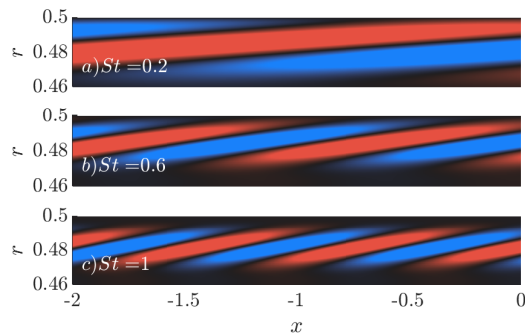


Figure 21: Spatial reconstruction of the optimal forcing modes for phase speed associated with the largest gain.

V. Conclusions

We have explored the dynamics of a turbulent nozzle boundary layer of a $M=0.4$ turbulent jet using high-fidelity LES. There were three goals: (1) to establish whether or not these dynamics are coupled to those of wavepackets in the jet; (2) to characterise the associated flow structures; and, (3) to propose a modelling framework.

SPOD was used to educe axisymmetric wavepackets both upstream and downstream of the jet exit plane. The analysis shows that the modes that optimally describe the downstream dynamics are coupled with the most energetic axisymmetric nozzle boundary-layer structures (NBL). The NBL structures educed using SPOD are tilted against the mean flow in the upstream regions, and rotate into the mean as they evolve towards the nozzle exit plane. This Orr-like behaviour is further confirmed by a radial velocity fluctuation that grows and then decays.

We perform a local stability analysis of the turbulent mean flow and find, by projecting the SPOD mode on a rank-1, '*Rank-BLB*' and '*Rank-BLB+FS*', truncations of the eigenbasis, that the salient traits of the NBL structures can be captured by the '*Rank-BLB*' truncation, comprised of modes of the boundary layer branch of the eigenspectrum. This further confirms the non-modal character of the educed structures.

This suggests the use of a resolvent framework for modelling of the dynamics, and so we perform a locally parallel resolvent analysis. This shows that the essential features of the educed NBL structures can be described by a small number of optimal resolvent response modes. The associated forcing is found, again consistent with the Orr mechanism, to be inclined against the mean flow.

Acknowledgements

The LES studies were supported by NAVAIR SBIR project under the supervision of J. T. Spyropoulos, with computational resources provided by DoD HPCMP at the ERDC DSRC supercomputer facility. OK would like to thank Leandra I. Abreu, who provided the script of velocity function to fit the LES flow.

References

- ¹Kaplan, O., Jordan, P., and Cavalieri, A. V., “Exploring the link between nozzle dynamics and wavepackets in a Mach 0.9 turbulent jet,” *23rd AIAA/CEAS Aeroacoustics Conference*, 2017, p. 3708.
- ²Jordan, P. and Colonius, T., “Wave packets and turbulent jet noise,” *Annual review of fluid mechanics*, Vol. 45, 2013, pp. 173–195.
- ³Cavalieri, A. V., Jordan, P., Colonius, T., and Gervais, Y., “Axisymmetric superdirectivity in subsonic jets,” *Journal of fluid Mechanics*, Vol. 704, 2012, pp. 388–420.
- ⁴Cavalieri, A. V., Rodríguez, D., Jordan, P., Colonius, T., and Gervais, Y., “Wavepackets in the velocity field of turbulent jets,” *Journal of fluid mechanics*, Vol. 730, 2013, pp. 559–592.
- ⁵Cavalieri, A. V., Jordan, P., and Lesshafft, L., “Wave-packet models for jet dynamics and sound radiation,” *Applied Mechanics Reviews*, Vol. 71, No. 2, 2019, pp. 020802.
- ⁶Schmidt, O. T., Towne, A., Colonius, T., Cavalieri, A. V., Jordan, P., and Brès, G. A., “Wavepackets and trapped acoustic modes in a turbulent jet: coherent structure eduction and global stability,” *Journal of Fluid Mechanics*, Vol. 825, 2017, pp. 1153–1181.
- ⁷Semeraro, O., Lesshafft, L., Jaunet, V., and Jordan, P., “Modeling of coherent structures in a turbulent jet as global linear instability wavepackets: Theory and experiment,” *International Journal of Heat and Fluid Flow*, Vol. 62, 2016, pp. 24–32.
- ⁸Fontaine, R. A., Elliott, G. S., Austin, J. M., and Freund, J. B., “Very near-nozzle shear-layer turbulence and jet noise,” *Journal of Fluid Mechanics*, Vol. 770, 2015, pp. 27–51.
- ⁹Brès, G. A., Jordan, P., Jaunet, V., Le Rallic, M., Cavalieri, A. V., Towne, A., Lele, S. K., Colonius, T., and Schmidt, O. T., “Importance of the nozzle-exit boundary-layer state in subsonic turbulent jets,” *Journal of Fluid Mechanics*, Vol. 851, 2018, pp. 83–124.
- ¹⁰Lumley, J. L., “The structure of inhomogeneous turbulent flows,” *Atmospheric turbulence and radio wave propagation*, 1967.
- ¹¹Citriniti, J. and George, W. K., “Reconstruction of the global velocity field in the axisymmetric mixing layer utilizing the proper orthogonal decomposition,” *Journal of Fluid Mechanics*, Vol. 418, 2000, pp. 137–166.
- ¹²Freund, J. and Colonius, T., “Turbulence and sound-field POD analysis of a turbulent jet,” *International Journal of Aeroacoustics*, Vol. 8, No. 4, 2009, pp. 337–354.
- ¹³Sinha, A., Rodríguez, D., Brès, G. A., and Colonius, T., “Wavepacket models for supersonic jet noise,” *Journal of Fluid Mechanics*, Vol. 742, 2014, pp. 71–95.
- ¹⁴Towne, A., Schmidt, O. T., and Colonius, T., “Spectral proper orthogonal decomposition and its relationship to dynamic mode decomposition and resolvent analysis,” *Journal of Fluid Mechanics*, Vol. 847, 2018, pp. 821–867.
- ¹⁵Brès, G. A., Ham, F. E., Nichols, J. W., and Lele, S. K., “Unstructured large-eddy simulations of supersonic jets,” *AIAA journal*, 2017, pp. 1164–1184.
- ¹⁶Chu, B.-T., “On the energy transfer to small disturbances in fluid flow (Part I),” *Acta Mechanica*, Vol. 1, No. 3, 1965, pp. 215–234.
- ¹⁷Rodríguez, D., Cavalieri, A. V., Colonius, T., and Jordan, P., “A study of linear wavepacket models for subsonic turbulent jets using local eigenmode decomposition of PIV data,” *European Journal of Mechanics-B/Fluids*, Vol. 49, 2015, pp. 308–321.
- ¹⁸Monkewitz, P. A., Chauhan, K. A., and Nagib, H. M., “Self-consistent high-Reynolds-number asymptotics for zero-pressure-gradient turbulent boundary layers,” *Physics of Fluids*, Vol. 19, No. 11, 2007, pp. 115101.
- ¹⁹Österlund, J. M., Johansson, A. V., Nagib, H. M., and Hites, M. H., “A note on the overlap region in turbulent boundary layers,” *Physics of Fluids*, Vol. 12, No. 1, 2000, pp. 1–4.
- ²⁰Cossu, C., Pujals, G., and Depardon, S., “Optimal transient growth and very large-scale structures in turbulent boundary layers,” *Journal of Fluid Mechanics*, Vol. 619, 2009, pp. 79–94.
- ²¹Passaglia, P.-Y., Ehrenstein, U., and Gallaire, F., “Control of a separated boundary layer: model reduction using global modes revisited,” *4th Global Instability and Control Symposium*, 2009, pp. CD-ROM.
- ²²Alizard, F. and Robinet, J.-C., “Modeling of optimal perturbations in flat plate boundary layer using global modes: benefits and limits,” *Theoretical and Computational Fluid Dynamics*, Vol. 25, No. 1-4, 2011, pp. 147–165.
- ²³Abreu, L. I., Cavalieri, A. V., and Wolf, W., “Coherent hydrodynamic waves and trailing-edge noise,” *23rd AIAA/CEAS Aeroacoustics Conference*, 2017, p. 3173.
- ²⁴Lesshafft, L., Semeraro, O., Jaunet, V., Cavalieri, A. V., and Jordan, P., “Resolvent-based modelling of coherent wavepackets in a turbulent jet,” *arXiv preprint arXiv:1810.09340*, 2018.
- ²⁵Kovesi, P., “Good colour maps: How to design them,” *arXiv preprint arXiv:1509.03700*, 2015.
- ²⁶Tissot, G., Lajús Jr, F. C., Cavalieri, A. V., and Jordan, P., “Wave packets and Orr mechanism in turbulent jets,” *Physical Review Fluids*, Vol. 2, No. 9, 2017, pp. 093901.
- ²⁷Jiménez, J., “How linear is wall-bounded turbulence?” *Physics of Fluids*, Vol. 25, No. 11, 2013, pp. 110814.